The Astrophysical Journal, 781:76 (8pp), 2014 February 1 doi:10.1088/0004-637X/781/2/76

WEAK TURBULENCE CASCADING EFFECTS IN THE ACCELERATION AND HEATING OF IONS IN THE SOLAR WIND

P. S. Moya[1,2], R. Navarro[3], A. F. Viñas[1], V. Muñoz[3], and J. A. Valdivia[3,4]
[1] NASA Goddard Space Flight Center, Heliophysics Science Division, Geospace Physics Laboratory, Mail Code 673, Greenbelt, MD 20771, USA; pablo.s.moyafuentes@nasa.gov
[2] Department of Physics, Catholic University of America, Washington, DC 20064, USA
[3] Departamento de Física, Facultad de Ciencias, Universidad de Chile, Las Palmeras 3425, Casilla 653, Santiago, Chile
[4] Centro para el Desarrollo de la Nanociencia y Nanotecnología, CEDENNA, Chile
Received 2013 June 14; accepted 2013 December 6; published 2014 January 10

ABSTRACT

We study the wave–particle interaction and the evolution of electromagnetic waves propagating through a solar-wind-like plasma composed of cold electrons, isotropic protons, and a small portion of drifting anisotropic He^{+2} ($T_{\perp\alpha} = 6\,T_{\parallel\alpha}$) and O^{+6} ($T_{\perp O} = 11\,T_{\parallel O}$) ions as suggested in Gomberoff & Valdivia and Gomberoff et al., using two approaches. First, we use quasilinear kinetic theory to study the energy transfer between waves and particles, with the subsequent acceleration and heating of ions. Second, 1.5 D (one spatial dimension and three dimensions in velocity space) hybrid numerical simulations are performed to investigate the fully nonlinear evolution of this wave–particle interaction. Numerical results of both approaches show that the temperatures of all species evolve anisotropically, consistent with the time-dependent wave-spectrum energy. In a cascade effect, we observe the emergence of modes at frequencies higher than those initially considered, peaking at values close to the resonance frequencies of O^{+6} ions ($\omega \sim \Omega_{cO}$) and He^{+2} ions ($\omega \sim \Omega_{c\alpha}$), being the peak due to O^{+6} ions about three times bigger than the peak associated with He^{+2} ions. Both the heating of the plasma and the energy cascade were more efficient in the nonlinear analysis than in the quasilinear one. These results suggest that this energy cascade mechanism may participate in the acceleration and heating of the solar wind plasma close to the Sun during fast streams associated with coronal holes.

Key words: acceleration of particles – methods: numerical – plasmas – solar wind – turbulence – waves

1. INTRODUCTION

The problem of the acceleration and heating of minor ions in the solar wind has been an interesting topic that has received special attention during the last few decades, especially related to the so-called fast solar wind (Axford & McKenzie 1992, 1996). Recent observations and theoretical results seem to indicate that most of the acceleration process occurs within a few solar radii from the Sun and that the main mechanism is due to Alfvén waves (Kohl et al. 1998; Cranmer et al. 1999a, 1999b; Esser et al. 1999; Tu & Marsch 1999; Marsch 1998; Hu & Habbal 1999; Cranmer 2002), probably through the resonant absorption of ion-cyclotron waves (Cranmer 2002; Isenberg 2001; Hollweg & Isenberg 2002; Kasper et al. 2013; Moya et al. 2013). However, the detailed processes for the energy transfer between waves and different particle species are still an open question.

Gomberoff & Valdivia (2002, 2003) and Gomberoff et al. (2004) have shown that the presence of heavy ions (for example, He^{+2}, O^{+5}, and Mg^{+9}; Esser et al. 1999; Kohl et al. 1999) with thermal anisotropy and drift velocities, with respect to the proton stream, are capable of generating ion-cyclotron waves beyond their respective gyrofrequencies. In a cascade-type effect (Chandran 2008; Luo & Melrose 2007), these waves can heat and accelerate less massive ions, which in turn may generate higher frequency instabilities and finally accelerate and heat protons. More recently, Moya et al. (2012), using quasilinear theory (Davidson & Ogden 1975; Krall & Trivelpiece 1986; Alexandrov et al. 1984; Dusenbery & Hollweg 1981; Yoon 1992; Marsch & Tu 2001; Yoon et al. 2003; Isenberg & Vasquez 2007) and hybrid simulations (Gary et al. 1997, 2000, 2001, 2003; Daughton et al. 1999; Ofman et al. 2001, 2011; Araneda et al. 2002; Ofman & Viñas 2007), studied the nonlinear wave–particle interaction between an electron–proton plasma and circularly polarized electromagnetic waves, propagating parallel along the magnetic field, through nonlinear, quasilinear theoretical models and hybrid computational simulations approaches. Numerical results show that both methods qualitatively agree in the evolution of the macroscopic plasma parameters.

Also, in Moya et al. (2011) it has been shown that the existence of a minor fraction of He^{+2} ions, with thermal anisotropy and drifting, with respect to a proton background in the direction of an ambient magnetic field, triggers an energy cascade from low to high modes, peaking at a particular frequency close to the ion resonance. All of these results seem to suggest that this energy cascade mechanism may participate in the acceleration and heating of the solar wind plasma close to the Sun. In this paper, we will study the relevance of this process for a thermal plasma composed of three ions species, where the predicted cascade should become more pronounced (Gomberoff & Valdivia 2003). Thus, to improve our study of the energy cascade process mentioned above, in this work we extend the nonlinear analysis, done for protons (Moya et al. 2012) and protons and alpha particles (Moya et al. 2011), to include O^{+6} ions as a third ion species.

First, we use the quasilinear theory for a thermal plasma that requires numerically solving the exact dispersion relation (Gomberoff et al. 2004), to have a better understanding of the energy cascade in which there is a transfer of wave energy from longer to shorter wave modes, with the subsequent acceleration of ions with an increasing q/m (charge over mass) ratio. Second, we perform one-dimensional hybrid simulations of the same system, in order to investigate the long term evolution of the full nonlinear wave–particle interaction in a three species cascade

process. All of these effects (energy cascade and nonlinear wave–particle interaction) are included in the study to show how the shape of the ion velocity distribution functions is controlled and regulated in the solar wind.

Further studies of the solar wind turbulence in the neighborhood of the break of the inertial range spectra as a function of wave vector **k**, with components parallel ($k_\parallel$) and perpendicular ($k_\perp$) to the magnetic field, revealed that the fluctuation spectrum is anisotropic and that the index of the power law distribution sometimes is greater at quasi-perpendicular wave vectors ($k_\perp \gg k_\parallel$) (Matthaeus et al. 1990; Horbury et al. 2005; Dasso et al. 2005) than at quasi-parallel propagation ($k_\parallel \gg k_\perp$). However, at very long wavelengths (smaller $|\mathbf{k}|$), there is still enough energy available for the quasi-parallel propagating waves to dominate the oblique wave modes (where $k_\parallel \gg k_\perp$) (Matthaeus et al. 1990, 1996a, 1996b; Leamon et al. 2000; Smith et al. 2001, 2006; Horbury et al. 2005, 2008; Bale et al. 2005, 2009), so that we have focused our research on this part of the wave spectrum range.

This article is organized as follows. In Section 2, we show the basic equations of quasilinear theory for the evolution of the macroscopic parameters of the distribution function, and we present numerical results for the case of circularly polarized electromagnetic waves propagating parallel to an ambient magnetic field, through a plasma composed of electrons, protons, and a minor percentage of drifting He^{+2} and O^{+6} ions with thermal anisotropy. In Section 3, we present the equations and results for the same problem as in Section 2, but using one-dimensional hybrid simulations. Finally, in Section 4, we compare the results of previous sections and summarize the conclusions of this article.

2. QUASILINEAR APPROXIMATION

2.1. Dispersion Relation

We consider a plasma in an external magnetic field $\mathbf{B_0} = B_0\hat{z}$, composed of electrons and several ions species drifting with respect to a fixed frame (the "Lab" frame) along the background magnetic field. Each species, labeled with index μ, has a drift velocity V_μ, mass m_μ, charge state z_μ, and density n_μ. To keep neutrality (zero net charge) and quasineutrality (current-free system), in our analysis we have subgroups of electrons canceling each ion species. Therefore, density and drift speed for each electron subgroup depends on the density and drift speed of the corresponding ion species.

The normalized dispersion relation for ion-cyclotron waves of frequency ω_k and wavenumber k, propagating parallel to the external magnetic field, assuming a bi-Maxwellian distribution function for each ion species, is (Gomberoff & Elgueta 1991; Astudillo 1996; Gomberoff & Valdivia 2002, 2003; Gomberoff et al. 2004; Moya et al. 2011)

$$y^2 = \sum_\mu z_\mu M_\mu \eta_\mu \times \left[A_\mu + \frac{[(A_\mu + 1)(x_y \pm M_\mu - yU_\mu) \mp M_\mu]}{y\delta_{\mu\parallel}} Z(\varphi_\mu) \right], \quad (1)$$

where the sign + (−) corresponds to right-handed (left-handed) polarization. In Equation (1), $x_y = \omega_k/\Omega_p$ and $y = ck/\omega_{pp}$ (where $\Omega_p = eB_0/m_pc$ is the proton cyclotron frequency, $\omega_{pp} = (4\pi n_p e^2/m_p)^{1/2}$ is the proton plasma frequency, e is the proton charge, and c is the speed of light); $U_\mu = V_\mu/V_{Ap}$ is the normalized drift speed, where $V_{Ap} = B_0/\sqrt{4\pi n_p m_p}$ is the proton Alfvén velocity; $M_\mu = z_\mu m_p/m_\mu$, and $\eta_\mu = n_\mu/n_p$. The plasma dispersion function (Fried & Conte 1961) Z is defined as

$$Z(\zeta) = \frac{1}{\sqrt{\pi}} \int_{-\infty}^{\infty} \frac{e^{-t^2}}{t - \zeta}\, dt,$$

where $\varphi_\mu = (x_y \pm M_\mu - yU_\mu)/y\delta_{\mu\parallel}$, $\delta_{\mu j} = v_{\mathrm{th},\mu,j}/V_{Ap}$, where $v_{\mathrm{th},\mu,j} = (2K_BT_{\mu j}/m_\mu)^{1/2}$ is the parallel ($j = \parallel$) and perpendicular ($j = \perp$) thermal velocity of the μth species, and K_B is the Boltzmann constant. Finally, we define $A_\mu = T_{\mu\perp}/T_{\mu\parallel} - 1 = \delta^2_{\mu\perp}/\delta^2_{\mu\parallel} - 1$ as the thermal anisotropy for the μth species.

Due to their small mass, we shall assume electrons as cold. Therefore, for electrons, the argument of the Z function is much larger than one and we approximate $Z(\varphi_e) \cong -1/\varphi_e$. Thus, for a solar-wind-like plasma composed of protons ($M_p = z_p = 1$); alpha particles ($M_\alpha \sim 0.5$, $z_\alpha = 2$); O^{+6} ions ($M_O \sim 0.375$, $z_O = 6$); and cold electrons, the warm dispersion relation can be written as

$$y^2 = \sum_i z_i M_i \eta_i \left[A_i \pm \frac{x_y - yU_i}{M_i} + \frac{[(A_i + 1)(x_y \pm M_i - yU_i) \mp M_i]}{y\delta_{i\parallel}} Z(\varphi_i) \right], \quad (2)$$

where the sum in i is now over all ion species ($i = p, \alpha, O$). In Equations (1) and (2) we have considered low frequencies, such that we can neglect the displacement current, and have accounted for each subgroup of electrons.

We consider typical solar wind parameters such as $\eta_\alpha \sim 0.05$ (Kamide & Chian 2007; Aschwanden 2006) for He^{+2} ions, and $\eta_O \sim 7 \times 10^{-4}$ (von Steiger et al. 2010) for O^{+6} ions. Remote sensing observations of the solar corona have shown that there is a preferential perpendicular heating of ion species, with anisotropy $A_p \sim 4$ for protons and $A_O \sim 10$ for O^{+5} ions, and also a preferential acceleration of heavy ions with respect to the protons (see, for example, Cranmer 2009 and references therein). Typical ions speeds at about 3 solar radii from the Sun are $U_O \sim 500$ km s^{-1} for O^{+5} ions, and $U_p \sim 300$ km s^{-1} for protons, so that the drift velocity between heavy ions and protons are of the order of a fraction of the local Alfvén speed $V_{Ap} \sim 700$ km s^{-1} (Cranmer 2009). Thus, in order to set up a situation similar as in collisionless coronal holes fast streams, we select the plasma parameters shown in Table 1 as the initial condition.

Table 1
Initial Normalized Plasma Parameters[a]

Species	η_μ	U_μ	$\delta^2_{\parallel\mu}$	A_μ
H^+	1	0	0.001	0
He^{+2}	5×10^{-2}	0.13	0.004	5
O^{+6}	7×10^{-4}	0.24	0.016	10

Note. Quasilinear and hybrid simulations.

Instead of considering O^{+5} ions that have been measured by remote sensing near the Sun (Kohl et al. 1998, 1999; Esser et al. 1999; Cranmer et al. 1999a, 1999b; Cranmer 2002), we use O^{+6} ions because they are about 100 times more abundant (Cranmer 2009). Also, since oxygen charge states freeze-in close to the Sun, where the wind is collisionless, the abundance of O^{+6} ions observed in situ between 1.3 and 5.4 AU (von Steiger et al.

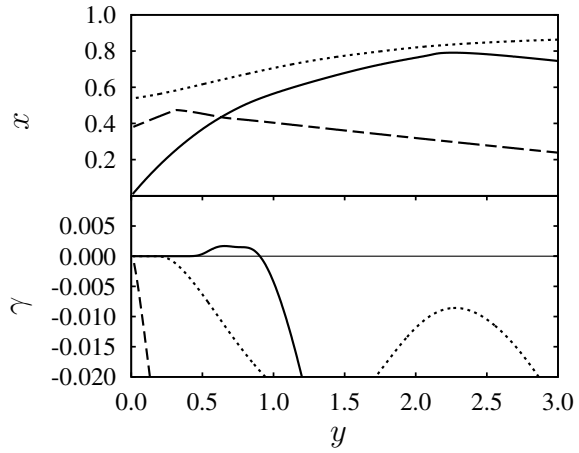

Figure 1. Numerical solutions of the linear dispersion relation (Equation (2)). Solid, dashed, and dotted curves correspond to the three principal branches for drift speeds, $\delta_\parallel$ and anisotropies given by Table 1. Top: normalized real frequencies x as a function of normalized wavenumber y. Bottom: normalized growth (damping) rates γ as a function of normalized wavenumber y for the corresponding branches in top panel.

2010) should not be different to the one found closer to the Sun in fast streams associated with coronal holes. Therefore, in order to more clearly illustrate the cascading effect, we are assuming that the O^{+6} ions, as the O^{+5} ions, also have a large thermal anisotropy and differential streaming which, to the best of our knowledge, have not yet been measured.

With regards to the alpha particles, in situ observations of fast wind streams protons and He^{+2} at 0.29 AU show that He^{+2} ions exhibit thermal anisotropies, being the anisotropy larger for measurements corresponding to the perihelion of the spacecraft (Marsch et al. 1982a, 1982b; Marsch 2006; Cranmer et al. 2009). The same kind of measurements show a preferential acceleration of the alpha particles in fast streams associated with coronal holes. Thus, it is reasonable to consider that the same ion populations may have similar (or even larger) thermal anisotropies and bulk velocities. Thereby, we are also assuming that He^{+2} ions also have a large thermal anisotropy and differential streaming with respect to the proton background, although, to the best of our knowledge, this has not yet been measured. In the near future, missions like NASA's Solar Probe+ and ESA's Solar Orbiter will offer measurements inside this region that will likely improve our understanding of solar wind acceleration and will help us to further validate our model.

In this work, we intend to study the acceleration and heating of ions through the time evolution of U_μ, $\delta_{\mu\parallel}$, and $\delta_{\mu\perp}$. In order to solve the warm dispersion relation (Equation (2)), we define $x_y = x + i\gamma$, where x is the real frequency of the mode and γ its growth rate, and solve for x and γ. The numerical solutions for the parameters chosen in Table 1 are shown in Figure 1. Let us note that none of the ion species satisfy the semi-cold approximation, and we are required to solve the problem for a thermal plasma using the Z function, which is an improvement from previous analysis (Moya et al. 2011, 2012). In Figure 1 (top), the solid, dashed, and dotted lines correspond to the three principal branches, namely, the O^{+6}-Alfvén branch, the He^{+2}-Alfvén branch, and the H^+-Alfvén branch, respectively. In addition, Figure 1(bottom) shows the corresponding growth rates $\gamma(y)$. For $y > 0$, in the case of the O^{+6}-Alfvén branch, it is observed that $\gamma(y)$ is positive only in a narrow region near $y = 0.7$ which corresponds to the instability region due to the combination between ions drifts and thermal anisotropy. Also, for $y \sim 1.1$ the growth rate becomes negative due to the resonant absorption of protons near their Doppler-shifted gyrofrequency. Depending on the magnetic field energy spectrum, these two contrary effects will compete to change the shape of the distribution function.

2.2. Temporal Evolution of Macroscopic Parameters

Assuming that the zeroth order distribution function varies slowly compared to the wave timescale, the temporal evolution equation of the μth species distribution function $f_{\mu 0}$, in the quasilinear approximation is given by (Krall & Trivelpiece 1986; Alexandrov et al. 1984)

$$\frac{\partial f_{\mu 0}}{\partial t} = -M_\mu \frac{e}{m_p} \int_{-\infty}^{\infty} dk \left(\mathbf{E}_{-\mathbf{k}} + \frac{1}{c}\mathbf{v} \times \mathbf{B}_{-\mathbf{k}} \right) \cdot \frac{\partial f_{\mu k}}{\partial \mathbf{v}}, \quad (3)$$

where $f_{\mu k}$ is the Fourier first order perturbation of the distribution function, with $\mathbf{E}_\mathbf{k}$ and $\mathbf{B}_\mathbf{k}$ as the Fourier electric and magnetic field spectra, respectively.

Using this expression, and taking moments of $f_{\mu 0}$, we can write a set of ordinary differential equations for all of the macroscopic parameters of the equilibrium distribution function, given by (Moya et al. 2011, 2012)

$$\frac{dU_\mu}{d\tau} = K_1^\mu(\tau), \quad (4)$$

$$\frac{d\delta_{\mu\parallel}}{d\tau} = \frac{1}{\delta_{\mu\parallel}(\tau)} K_{2\parallel}^\mu(\tau) - 2\frac{U_\mu(\tau)}{\delta_{\mu\parallel}(\tau)} K_1^\mu(\tau), \quad (5)$$

$$\frac{d\delta_{\mu\perp}}{d\tau} = \frac{1}{2\delta_{\mu\perp}(\tau)} K_{2\perp}^\mu(\tau), \quad (6)$$

where $\tau = \Omega_p t$, and K_1^μ, $K_{2\parallel}^\mu$ and $K_{2\perp}^\mu$ are nonlinear functions of time that must be solved simultaneously with the dispersion relation and the evolution of the magnetic field spectral energy $|B_k|^2$ (see the Appendix). In this approximation, the time evolution of $|B_k|^2$ is given by

$$\frac{\partial \varepsilon_y}{\partial \tau} = 2\,\gamma\,\varepsilon_y, \quad (7)$$

where

$$\varepsilon_y = \frac{\omega_{pp}}{c} \frac{1}{2\pi L} \frac{|B_k|^2}{B_0^2}, \quad (8)$$

and L is the reference length of the plasma, which is of the order of several proton inertial lengths. In the case of hybrid simulations (explained in Section 3), L corresponds to the length of the simulation box. It is important to mention that in all the equations, we have both the real and imaginary part of the complex frequency (see the Appendix). To solve the systems (Equations (4)–(7)) we need to explicitly solve the dispersion relation (Equation (2)).

2.3. Numerical Results

To solve the system of quasilinear equations, we use a discrete grid in the normalized wavenumber y space with 600 points between $-3 < y < 3$. Hence, the separation between points is $dy = 0.01$. The time step is chosen to be $d\tau = 0.025$. Knowing the magnetic field spectrum and the value of the parameters at an instant in time τ, we can solve the dispersion relation to find the complex frequency x_y, as a function of y, at

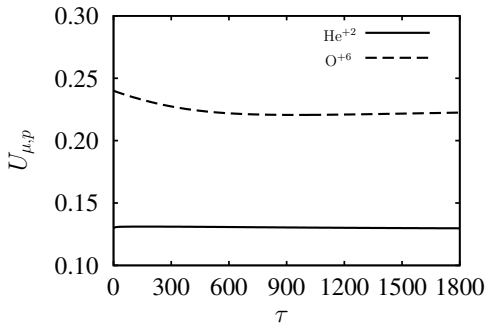

Figure 2. Quasilinear time evolution of the differential streamings $U_{\mu,p}$ between protons and He^{+2} ($\mu = \alpha$, solid) ions, and protons and O^{+6} ($\mu = O$, dashed). It can be seen that as time evolves, the decrease in the O^{+6} ions drift velocity produces a reduction in $U_{O,p}$ while the differential streaming between He^{+2} ions and protons $U_{\alpha,p}$ remains constant.

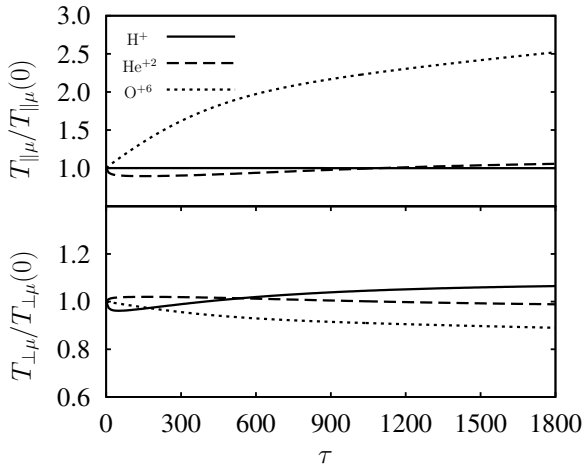

Figure 3. Top: parallel temperatures as a function of time for the quasilinear model with respect to their initial values. Solid, dashed, and dotted lines correspond to protons, He^{+2}, and O^{+6}, respectively. Bottom: the same as in the top panel but for perpendicular temperatures.

this particular time. Then, we calculate the integrals defined in the system of equations (Equations (4)–(7)), to evaluate the time derivative of each parameter for each species μ. We then use a fourth order Runge–Kutta method (García 2000) to evolve the whole system to the next time step $\tau + d\tau$. Numerical integration is performed until $\tau = 1800$. In the semi-cold approximation, for each wavenumber there are in general three values of x_y, corresponding to the three main left-handed branches of the dispersion relation (Gomberoff & Valdivia 2003; Gomberoff et al. 2004). In the case of a thermal plasma, considered in this manuscript, for each wavenumber there are, in general, many solutions for x_y, and all of them should be considered in Equations (4)–(7). However, it turns out that the cascading effect we are investigating is more evident for the O^{+6}-Alfvén branch, so in this manuscript we use this branch only. As we mentioned in Section 1, the emergence of ion-cyclotron instabilities in the dispersion relation is due to the combination of different ion species with thermal anisotropy and drift velocities between each other. For example, in the case of the particular chosen parameters (see Table 1), the existence of a drift between anisotropic O^{+6} and anisotropic He^{+2} triggers an instability associated with O^{+6}-Alfvén branch, with a maximum growth rate that depends strongly on the thermal anisotropies of both species, as well as the differential streaming between ions and the proton background (Gomberoff & Valdivia 2002, 2003; Gomberoff et al. 2004; Moya et al. 2011). If we had considered a different drift between O^{+6} and H^+, but we had chosen the same anisotropies and drift with respect to protons, we would have obtained a similar maximum growth rate for the instability associated with O^{+6}-Alfvén branch, but at a different wavenumber. For example, using the same parameters as in Table 1 and normalized drift speeds $U_O = 0$, $U_O = 0.12$, and $U_O = 0.24$ as in the manuscript, the maximum growth rate is $\gamma_{\max} \sim 0.002$ but occurs at $y \sim 0.35$, $y \sim 0.6$ and $y \sim 0.75$, respectively.

As an initial condition we use the same plasma parameters as in Figure 1 (see Table 1) and we choose a power law initial magnetic field spectrum given by

$$\varepsilon_y(t = 0) = 10^{-4}|y|^{-5/3}\,. \tag{9}$$

This profile for the initial magnetic energy spectrum was chosen to simulate a situation similar to those discussed in Horbury et al. (2005, 2008) and Bale et al. (2005, 2009) where most of the wave frequencies are below the proton gyrofrequency ($x = 1$). Figure 1(bottom) shows a region of unstable wavelengths (between $0.5 < y < 1$) in which waves will effectively interact with the heavy ions, triggering the cascade and the subsequent new high-frequency modes. Beyond this range ($y > 1$), the imaginary part of the frequencies becomes negative, suggesting proton heating due to resonant absorption as expected. It is important to emphasize that in the quasilinear approximation, the full temporal dependence of the macroscopic parameters of the distribution function depends strongly on the imaginary part of the frequency. This has been demonstrated in the semi-cold approximation (Moya et al. 2011, 2012), and shows the same behavior in the warm case (the present work). The plasma parameters used in Figure 1(bottom) yields a maximum growth rate of $\gamma_{\max} \sim 2 \times 10^{-3}$ which corresponds to a timescale of $500\,\Omega_p$. Thus, evolving the system until $\tau = 1800$ (1800 proton gyroperiods) should be long enough to observe significant quasilinear effects.

In Figure 2 we show the normalized differential streaming $U_{\mu,p}$ between minor ions and protons as a function of time. Due to the profile of $K_1^{\mu}(\tau)$ (Equation (A8)), in every time step, the total time derivative of U_α and U_p is essentially null (Moya et al. 2011, 2012) and the differential streaming $U_{\alpha,p}$ between these species does not change considerably so that it can be taken as a constant (see Figure 2). In contrast, for O^{+6} ions the situation is different. This species undergoes a decrease of its drift velocity, and also of $U_{O,p}$, before $\tau = 600$. Although there are no major changes in the differential streaming between species, the existence of an initial $U_{\mu,p} \neq 0$ is very important for the growth and damping rates. The unstable frequency region and the subsequent growth of the corresponding Alfvén waves are due to the combined effect of the thermal anisotropies and differential streaming of the heavy ions (Gomberoff & Elgueta 1991; Gomberoff & Valdivia 2002, 2003; Gomberoff et al. 2004), as mentioned in Section 1.

The temporal evolution of the temperatures for each species is shown in Figure 3. The parallel temperatures (top panel) show preferential heating of O^{+6} ions reaching values of $T_{\|O} \sim 2.5\,T_{\|O}(0)$ by the end of the time interval. The He^{+2} ions exhibit first a small cooling and then a small heating, while protons show no noticeable change since their parallel temperature remains almost constant. In contrast, Figure 3 (bottom) shows a perpendicular heating of protons (solid curve) reaching values of

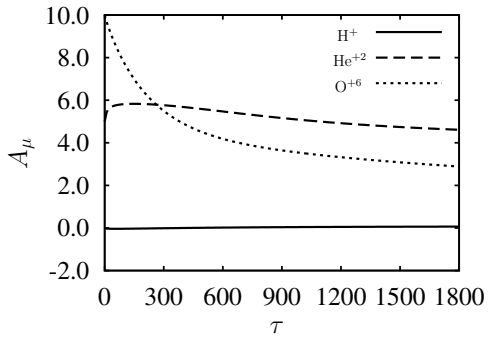

Figure 4. Temporal evolution of quasilinear thermal anisotropies for protons (solid), He^{+2} (dashed), and O^{+6} (dotted) ions.

$T_{\perp p} \sim 1.1\, T_{\perp p}(0)$ by the end of the time interval. Similarly, O^{+6} ions (dotted curve) exhibit a small perpendicular cooling of no more than 11% while the He^{+2} ions perpendicular temperature remains almost constant (dashed curve). Even though, based on observations, one would naively expect that the heating would be more intense for heavy ions, this behavior depends on the initial values of the thermal anisotropy of protons and ions. While protons contribute only with absorption (see Figure 1(bottom)), the initial thermal anisotropies of both ion species generate instabilities near $y \sim 0.75$ and trigger the energy cascade already mentioned (see Figure 5). All of these heating and cooling processes are anisotropic, thus there is a change in the thermal anisotropies. In Figure 4, the temporal evolution of the thermal anisotropies for each species is shown. In the case of O^{+6} ions (dotted lines), the large, initial anisotropy rapidly relaxes from $A_O(0) = 10$ to $A_O \sim 4$ before $\tau = 600$ (the same time interval in which its drift speed evolves), and then slowly continues to decrease until it reaches a value of $A_O \sim 2.9$ at the end of the simulation. He^{+2} ions, due to the initial parallel cooling, reach $A_\alpha \sim 5.9$ at $\tau \sim 200$, but then the anisotropy starts to relax, and by the end of the interval A_α reaches $A_\alpha \sim 4.6$. For protons, due to the anisotropic heating, the initial isotropic distribution function becomes slightly anisotropic with $A_p \sim 0.1$ at $\tau = 1800$. As time progresses, the quasilinear evolution saturates and it seems that the system is slowly approaching equilibrium. However, by $\tau = 1800$ it is not possible to draw definite conclusions about the complete behavior for longer times. We will see from the hybrid simulations described in the next section that at $\tau \sim 250$ some nonlinear processes, not described in the quasilinear approximation, start to become relevant.

Finally, the total free energy available due to the thermal anisotropy of the ions distribution functions is absorbed by the electromagnetic field to preserve the total energy of the system (Krall & Trivelpiece 1986; Moya et al. 2011). In Figure 5 we show the magnetic field energy spectrum near $y = 0.75$ (top panel) and $x = 0.4$ (bottom panel) for several time steps. The initial power law spectrum changes due to absorption and instability (emission) regions, as shown in Figure 1(bottom). Furthermore, Figure 5 shows the appearance of modes with frequencies larger than those existing in the initial spectrum at the expense of the initial thermal anisotropy of the minority species. Moreover, there are two significant peaks with frequencies near the ions gyrofrequencies $\omega = \Omega_\alpha$ ($x = 0.5$) and $\omega = \Omega_O$ ($x = 0.375$). The first frequency peak is less pronounced, which is due to the wave–particle interaction between the O^{+6}-Alfvén waves and He^{+2} population, and turned out to be absorbed at the end of the simulation. The second

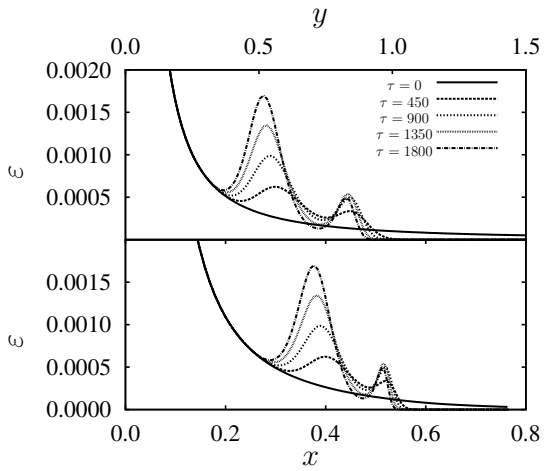

Figure 5. Normalized magnetic field energy spectrum for several times as a function of wavenumber (top panel) and frequency (bottom panel). We observe that as time advances there is an emergence of waves at higher modes (frequencies) compared to the initial ones, i.e., a wave cascade.

frequency peak near $x = 0.375$ is bigger and continues to grow until it reaches the end of the simulation. This is the main manifestation of the energy cascade from lower to higher electromagnetic wave modes. In summary, and for the initial set of parameters selected in this quasilinear approximation, the system evolves by transferring energy from the heavy ions to the waves and to the protons. This behavior slowly approaches an asymptotic state.

3. HYBRID MODEL

Due to the large difference in mass between electrons and protons, we use a hybrid model to describe the plasma system (i.e., which describes the ions kinetically while treating electrons as a fluid). These models have been widely used in the study of the self-consistent evolution of particles and fields, and the nonlinear wave–particle interaction in solar wind plasma (Gary et al. 1997, 2000, 2001, 2003; Daughton et al. 1999; Ofman et al. 2001, 2011; Araneda et al. 2002; Winske et al. 2003; Ofman & Viñas 2007). To compare with the quasilinear results shown in the previous section, we have performed numerical hybrid simulations in 1.5D (one spatial dimension, the x coordinate, and three dimensions in velocity space) for a plasma composed of electrons, protons, He^{+2}, and O^{+6} ions in the presence of a background magnetic field $\mathbf{B_0} = B_0\hat{x}$. Electrons are considered to be massless and isothermal (Moore et al. 1991; Gary et al. 2001; Ofman et al. 2001, 2011; Ofman & Viñas 2007). To solve for the electromagnetic fields, we impose periodic boundary conditions in x, with a box containing $N_x = 512$ cells of size $dx = 0.25$ with 800 particles per species per cell. We have chosen the same normalization as in the quasilinear case, and we have normalized the position in terms of the ion inertial length c/ω_{pp}. The particle and field equations were integrated in time using a rational Runge–Kutta method (Wambecq 1978), whereas the spatial derivatives are calculated by the pseudospectral fast Fourier transform method (Press et al. 1992), imposing periodic boundary conditions. To keep the same numerical accuracy of the quasilinear simulation, we choose a $d\tau$ smaller ($d\tau = 0.0125$) and we ran the simulation until $\tau = 500$. As in the quasilinear case, during the integration the total energy of the system remained constant to better than 5%.

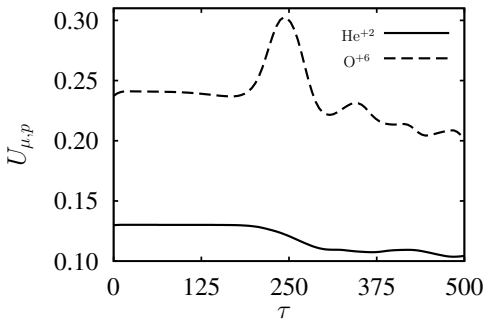

Figure 6. Hybrid differential streamings between protons and He^{+2} (solid) and O^{+6} (dashed) ions as a function of time. It can be seen that the time evolution is qualitatively similar to the quasilinear case (see Figure 2).

Our hybrid simulation is carried out in the electron reference frame. We impose quasineutrality and zero parallel current, with parallel drifts $U_p = -z_\alpha n_\alpha U_{\alpha,p} - z_O n_O U_{O,p}$ for protons; $U_\alpha = n_p U_{\alpha,p} - z_O n_O U_{O,\alpha}$ for He^{+2}; and $U_O = n_p U_{O,p} + z_\alpha n_\alpha U_{O,p}$ for O^{+6} ions. The variables $U_{i,j}$ are the normalized differential streaming between the ith and jth species ($i, j = p, \alpha, O$). In order to compare with the quasilinear case, we select the same parameters as in Table 1. Thus, we have $U_{\alpha,p} = 0.13$, $U_{O,p} = 0.24$, and $U_{O,\alpha} = 0.11$, all expressed in terms of local Alfvén speed. We use a bi-Maxwellian as the initial condition where the particle velocities were randomized and electrons were considered as cold. For these parameters, we have performed simulations using an initial electromagnetic fluctuation spectrum with 5% of maximum amplitude, with respect to B_0 and a power law spectral profile of $k^{-5/3}$, as in Equation (9). The hybrid and quasilinear simulations are performed in different frames, thus a Doppler shift in the frequencies is expected. However, our results show that the differential streaming between electrons and protons is small and therefore the Doppler shift is irrelevant.

3.1. Numerical Results

Figure 6 shows the normalized differential streaming $U_{\mu,p}$ between minor ions and protons. These results are different to those obtained in the quasilinear method. For He^{+2} ions (solid curve) there is a decrease (of about the 20%), of the initial differential streaming, being $U_{\alpha,p} = 0.1$ by $\tau = 500$. In contrast with the quasilinear case, O^{+6} ions (dashed curve) undergo a rapid increase of their drift speed and consequently $U_{O,p}$ increases from $U_{O,p} = 0.23$ at $\tau = 180$, to $U_{O,p} \sim 0.3$ at $\tau \sim 250$. Later, for $\tau > 250$, $U_{O,p}$ starts to decrease until $U_{O,p} \sim 0.2$ by the end of the simulation. This complex behavior may be due to nonlinear effects beyond the quasilinear approximation, such as wave–wave interaction, that produces momentum transfer between different species.

The evolution of the temperatures of each species is shown in Figure 7. For parallel temperatures (top panel) a preferential heating of O^{+6} ions is observed (dotted curve), while He^{+2} ions are slightly heated (dashed line). Furthermore, the heating of O^{+6} ions is similar to the quasilinear case, reaching $T_{\|O} \sim 4\, T_{\|O}(0)$ by the end of the simulation. Unlike the quasilinear case, the evolution of the proton parallel temperature (solid curve in Figure 7) shows a more significant heating than that of O^{+6} ions, with $T_{\|p} \sim 7\, T_{\|p}(0)$ by the end of the simulation ($\tau = 500$). It is important to note that although both protons and O^{+6} ions are heated in the parallel direction, the proton heating began 70 proton gyroperiods ($\tau \sim 250$) after the onset

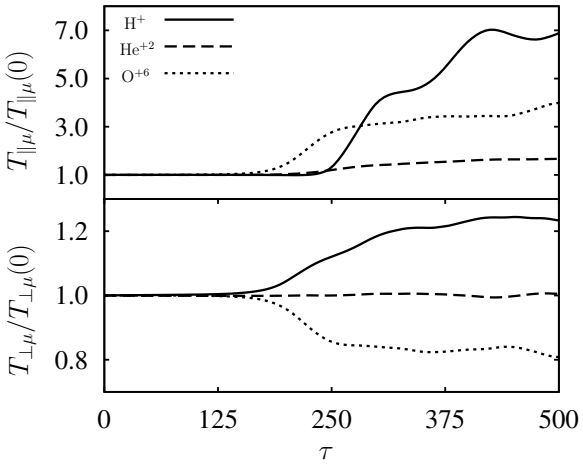

Figure 7. Top: parallel temperatures as a function of time in the hybrid simulations with respect to their initial values. Solid, dashed, and dotted lines correspond to protons, He^{+2}, and O^{+6}, respectively. Bottom: the same as in top panel but for perpendicular temperatures.

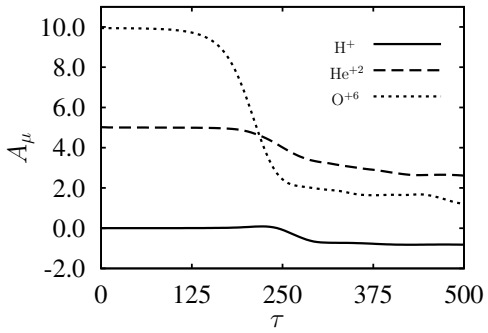

Figure 8. Thermal anisotropies for protons (solid), He^{+2} ions (dashed), and O^{+6} ions (dotted) from hybrid simulations.

of O^{+6} ions heating ($\tau \sim 180$). This is a nonlinear behavior that is absent in the quasilinear theory (Yoon et al. 2003), which produces the excitation of modes in other branches through wave–wave interaction. This result clearly shows an energy cascading effect in which the heavy ions interact with waves at longer wavelengths, driving instabilities and then transferring the energy to protons at shorter wavelengths.

The evolution of the perpendicular temperatures is shown at the bottom panel of Figure 7. The figure shows a perpendicular heating of protons (solid curve), reaching a value of $T_{\perp p} \sim 1.2\, T_{\perp p}(0)$ by the end of the simulation, whereas O^{+6} ions (dotted curve) exhibit a perpendicular cooling of the same order (about 20%), while for He^{+2} ions the temperature remains constant (dashed curve). These results appear to be similar with the quasilinear case as shown in the bottom panel of Figure 3. The evolution of thermal anisotropies ($A_\mu = -1 + T_{\perp,\mu}/T_{\|,\mu}$) of each species is shown in Figure 8. The initially large O^{+6} anisotropy $A_O(0) = 10$ (dotted lines), rapidly relaxes to $A_O \sim 2$ by $\tau = 250$, and saturates with a value of $A_O \sim 1.2$ by $\tau = 500$. For He^{+2} ions (dashed curve), the anisotropy relaxes reaching a value of $A_\alpha \sim 2.6$ by the end of the simulation, whereas the proton anisotropy (solid line), which was initially isotropic, became anisotropic with $A_p \sim -0.8$ at $\tau = 500$.

In comparison with the quasilinear approximation (shown in Figure 4), the final negative proton thermal anisotropy in the hybrid model is related to nonlinear effects not included in the quasilinear approximation. Our results indicate no

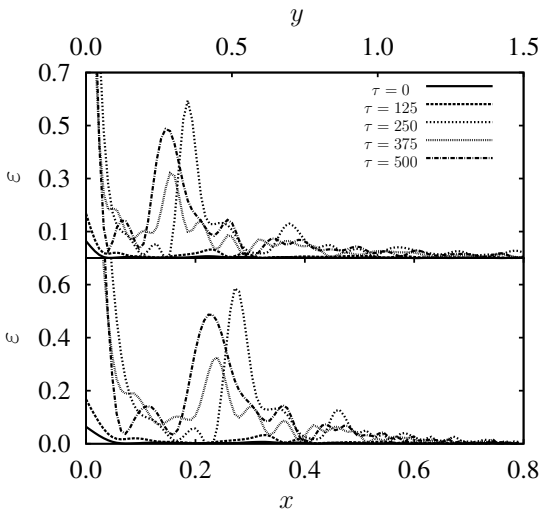

Figure 9. Magnetic field fast Fourier transform energy spectrum for several times as a function of wavenumber (top panel) and frequency (bottom panel) in the hybrid simulations, in arbitrary units. We observe the same energy cascade as in the quasilinear solution (see Figure 5), but the change is more pronounced.

significant differences in the evolution of He^{+2} and O^{+6} thermal anisotropies when we compare both the quasilinear model and the hybrid simulations. In summary, our results show a qualitative agreement between quasilinear and hybrid simulations.

The time evolution of the macroscopic parameters of the plasma influences the excitation and absorption of electromagnetic waves. In Figure 9 we show the magnetic field energy spectrum near $y = 0.75$ (top panel) or $x = 0.4$ (bottom panel) at different times in the simulation. As in the quasilinear solutions, the initial power law spectrum evolves due to wave–particle interaction. The figure shows the emergence of modes with frequencies larger than those existing in the initial spectrum, as in the quasilinear case (see Figure 5). There are two significant peaks at frequencies near the ions gyrofrequencies $\omega = \Omega_\alpha$ ($x = 0.5$) and $\omega = \Omega_O$ ($x = 0.35$). The less pronounced peak is due to the wave–particle interaction with the He^{+2} population, while the second peak, which is about three times bigger near $x = 0.35$, is due to wave–particle interaction with O^{+6} ions. Compared with the quasilinear case, both peaks become larger and more relevant, but start to dampen by the second half of the simulation, particularly the one associated with He^{+2} ions resonance. Finally, differences between both methods are related to nonlinear effects such as mode coupling (Yoon et al. 2003), Landau damping (Vasquez & Hollweg 1999; Buti et al. 2000), and parametric decays (Viñas & Goldstein 1991; Agim et al. 1995; Araneda et al. 2008; Verscharen et al. 2012). Nevertheless, the resulting energy cascade effect, from lower to higher electromagnetic modes, is present in the hybrid simulations, being more evident and efficient than in the quasilinear description.

4. DISCUSSION AND CONCLUSIONS

We have studied the nonlinear wave–particle interaction in a solar-wind-like plasma from two complementary kinetic approaches, based on quasilinear theory and hybrid models. The results obtained here allow us to compare the basic properties of the resonant wave–particle interaction using these different self-consistent nonlinear models.

Our results indicate that both the quasilinear and the hybrid simulations show that heating occurs in the perpendicular temperature of protons and parallel temperature of O^{+6} ions. However, the hybrid simulations show stronger parallel heating of the protons than in the quasilinear one. Both methods agree in that for He^{+2} ions, the evolution of the temperatures was small with a slight perpendicular cooling in the quasilinear, but a small heating in the hybrid case. All of these differences are related to the absence of higher order nonlinear effects in the quasilinear theory, which are present in the hybrid, fully nonlinear simulations. In summary, both models agree on the evolution of the differential streaming between protons and minor ions, and they further agree on the evolution of the thermal anisotropy of minor ions.

With regards to the evolution of magnetic field spectrum, both models yield similar results, showing the cascading effect from lower to higher frequencies in agreement with previous work (Moya et al. 2011, 2012). The cascade effect appears as the emergence of higher frequencies modes, peaking at frequencies near the ions resonances, being stronger in the hybrid case than in quasilinear one (see Figures 5 and 9). Through this effect, it is clear that the heavier ions interact with waves, generating instabilities and transferring the energy to protons.

In conclusion, we have shown that the presence of minor populations of heavy ions, with thermal anisotropy and differential streaming with respect to the background protons, triggers an energy cascade from low to high frequencies close to each ion species gyroresonance, with the subsequent heating of ions with increasing q/m ratio. All of these results suggest that resonant absorption of ion-cyclotron waves, and this energy cascade mechanism, may be relevant in the acceleration and heating of the solar wind plasma close to the Sun during fast streams associated with coronal holes.

We give thanks to Comisión Nacional de Ciencia y Tecnología (CONICyT, Chile) for a Becas-Chile Postdoctoral Fellowship (PSM) and Doctoral Fellowship No. 21100691 (R.N.). We also acknowledge support from FONDECyT grants Nos. 1080658, 1110135, and 1110729 (J.A.V.) and No. 1121144 (V.M.). We also thank Cedenna for support.

APPENDIX

DETAILED QUASILINEAR THEORY

In quasilinear theory, the temporal evolution equation of the μth species distribution function $f_{\mu 0}$ is given by (Krall & Trivelpiece 1986; Alexandrov et al. 1984)

$$\frac{\partial f_{\mu 0}}{\partial t} = -M_\mu \frac{e}{m_p} \int_{-\infty}^{\infty} dk \left(\mathbf{E}_{-\mathbf{k}} + \frac{1}{c} \mathbf{v} \times \mathbf{B}_{-\mathbf{k}} \right) \cdot \frac{\partial f_{\mu k}}{\partial \mathbf{v}}, \quad \text{(A1)}$$

where $f_{\mu k}$ is the Fourier first order perturbation of the distribution function, with $\mathbf{E}_\mathbf{k}$ and $\mathbf{B}_\mathbf{k}$ as the Fourier electric and magnetic field spectra, respectively.

Taking moments of the distribution functions, we define

$$K_1^\mu(t) = \int v_z (\partial f_{\mu 0}/\partial t)\, d\mathbf{v}, \quad \text{(A2)}$$

$$K_{2\parallel}^\mu(t) = \int v_z^2 (\partial f_{\mu 0}/\partial t)\, d\mathbf{v}, \quad \text{(A3)}$$

$$K_{2\perp}^\mu(t) = \int v_\perp^2 (\partial f_{\mu 0}/\partial t)\, d\mathbf{v}, \quad \text{(A4)}$$

and writing a set ordinary of differential equations for all the parameters of the equilibrium distribution function, in terms of the normalized variables, we obtain (Moya et al. 2011, 2012)

$$\frac{dU_\mu}{d\tau} = K_1^\mu(\tau), \tag{A5}$$

$$\frac{d\delta_{\mu\parallel}}{d\tau} = \frac{1}{\delta_{\mu\parallel}(\tau)} K_{2\parallel}^\mu(\tau) - 2\frac{U_\mu(\tau)}{\delta_{\mu\parallel}(\tau)} K_1^\mu(\tau), \tag{A6}$$

$$\frac{d\delta_{\mu\perp}}{d\tau} = \frac{1}{2\delta_{\mu\perp}(\tau)} K_{2\perp}^\mu(\tau). \tag{A7}$$

In the case of bi-Maxwellian zeroth order distribution functions,

$$K_{1\parallel}^\mu(\tau) = -M_\mu^2 \int_{-\infty}^{\infty} dy \frac{\varepsilon_y}{y} \mathrm{Im}[\chi_\mu], \tag{A8}$$

$$K_{2\parallel}^\mu(\tau) = M_\mu^2 \int_{-\infty}^{\infty} dy \frac{\varepsilon_y}{y^2} \mathrm{Im}[x_y - yU_\mu + (x_y \pm M_\mu)\chi_\mu], \tag{A9}$$

$$K_{2\perp}^\mu(\tau) = -M_\mu^2 \int_{-\infty}^{\infty} dy \frac{\varepsilon_y}{y^2} \mathrm{Im}[x_y - yU_\mu + (x_y + x_{-y} \pm M_\mu)\chi_\mu], \tag{A10}$$

where

$$\chi_\mu = A_\mu + \frac{[A_\mu(x_y \pm M_\mu - yU_\mu) + x_y - yU_\mu]}{y\delta_{\mu\parallel}} Z(\phi_\mu), \tag{A11}$$

and ε_y is the normalized magnetic field spectral energy per unit of length.

REFERENCES

Agim, Y., Viñas, A. F., & Goldstein, M. L. 1995, JGR, 100, 17081
Alexandrov, A. F., Bogdankevich, L. S., & Rukhadze, A. A. 1984, Principles of Plasma Electrodynamics (Berlin: Springer)
Araneda, J. A., Marsch, E., & F.-Viñas, A. 2008, PhRvL, 100, 125003
Araneda, J. A., Viñas, A. F., & Astudillo, H. 2002, JGR, 107, 1453
Aschwanden, M. J. 2006, Physics of the Solar Corona. An Introduction with Problems and Solutions (Chichester, UK: Praxis)
Astudillo, H. F. 1996, JGR, 101, 24433
Axford, W. I., & McKenzie, J. F. 1992, in The Origin of the High Speed Solar Wind Streams (New York: Univ. Press), 1
Axford, W. I., & McKenzie, J. F. 1996, in AIP Conf. Proc., Solar Wind Eight (New York: Pergamon), 382
Bale, S. D., Kasper, J. C., Howes, G. G., et al. 2009, PhRvL, 103, 211101
Bale, S. D., Kellog, P. J., Mozer, F. S., Horbury, T. S., & Reme, H. 2005, PhRvL, 94, 215002
Buti, B., Velli, M., Liewer, P. C., Goldstein, B. E., & Hada, T. 2000, PhPl, 7, 3998
Chandran, B. G. D. 2008, PhRvL, 101, 235004
Cranmer, S. R. 2002, SSRv, 101, 229
Cranmer, S. R. 2009, LRSP, 6, 3
Cranmer, S. R., Field, G. B., & Kohl, J. L. 1999a, ApJ, 518, 481
Cranmer, S. R., Kohl, J. L., Noci, G., et al. 1999b, ApJ, 511, 481
Cranmer, S. R., Matthaeus, W. H., Breech, B. A., & Kasper, J. C. 2009, ApJ, 702, 1604
Dasso, S., Milano, L. J., Matthaeus, W. H., & Smith, C. W. 2005, ApJL, 635, L181
Daughton, W., Gary, P. S., & Winske, D. 1999, JGR, 104, 4657
Davidson, R. C., & Ogden, J. M. 1975, PhFl, 18, 1045
Dusenbery, P. B., & Hollweg, J. V. 1981, JGR, 86, 153
Esser, R., Fineschi, S., Dobrzycka, D., et al. 1999, ApJL, 510, L63
Fried, B. D., & Conte, S. D. 1961, The Plasma Dispersion Function (San Diego, CA: Academic)
García, A. L. 2000, Numerical Methods for Physics (2nd ed.; Englewood Cliffs, NJ: Prentice-Hall)
Gary, P. S., Wang, J., Winske, D., & Fuselier, S. A. 1997, JGR, 102, 27159
Gary, S. P., Yin, D., Winske, D., & Ofman, L. 2001, JGR, 106, 10715
Gary, P. S., Yin, L., Winske, D., & Reisenfeld, D. B. 2000, GeoRL, 27, 1355
Gary, P. S., Yin, L., Winske, D., et al. 2003, JGR, 108, 1068
Gomberoff, L., & Elgueta, R. 1991, JGR, 96, 9801
Gomberoff, L., Muñoz, V., & Valdivia, J. A. 2004, P&SS, 52, 679
Gomberoff, L., & Valdivia, J. A. 2002, JGR, 107, 1494
Gomberoff, L., & Valdivia, J. A. 2003, JGR, 108, 1050
Hollweg, J. V., & Isenberg, P. A. 2002, JGR, 107, 1147
Horbury, T. S., Forman, M. A., & Oughton, S. 2005, PPCF, 47, B703
Horbury, T. S., Forman, M., & Oughton, S. 2008, PhRvL, 101, 175005
Hu, Y. Q., & Habbal, S. R. 1999, JGR, 104, 17045
Isenberg, P. A. 2001, JGR, 106, 29249
Isenberg, P. A., & Vasquez, B. J. 2007, ApJ, 668, 546
Kamide, Y., & Chian, A. C. L. (ed.) 2007, Handbook of the Solar-Terrestrial Environment (Berlin: Springer)
Kasper, J. C., Maruca, B. A., Stevens, M. L., & Zaslavsky, A. 2013, PhRvL, 110, 091102
Kohl, J. L., Esser, R., Cranmer, S. R., et al. 1999, ApJL, 510, L59
Kohl, J. L., Noci, G., Antonucci, E., et al. 1998, ApJL, 501, L127
Krall, N. A., & Trivelpiece, A. W. 1986, Principle of Plasma Physics (San Francisco, CA: San Francisco Press)
Leamon, R. J., Matthaeus, W. H., Smith, C. W., et al. 2000, ApJ, 537, 1054
Luo, Q., & Melrose, D. 2007, P&SS, 55, 2281
Marsch, E. 1998, NPGeo, 5, 11
Marsch, E. 2006, LRSP, 3, 1
Marsch, E., Mhlhuser, K.-H., Rosenbauer, H., Schwenn, R., & Neubauer, F. M. 1982a, JGR, 87, 35
Marsch, E., Mhlhuser, K.-H., Schwenn, R., et al. 1982b, JGR, 87, 52
Marsch, E., & Tu, C. Y. 2001, JGR, 106, 8357
Matthaeus, W. H., Ghosh, S., Oughton, S., & Roberts, D. A. 1996a, JGR, 101, 7619
Matthaeus, W. H., Goldstein, M. L., & Roberts, D. A. 1990, JGR, 95, 20673
Matthaeus, W. H., Zank, G. P., & Oughton, S. 1996b, JPlPh, 56, 659
Moore, K. R., Thomas, V. A., & McComas, D. J. 1991, JGR, 96, 7779
Moya, P. S., Muñoz, V., Rogan, J., & Valdivia, J. A. 2011, JASTP, 73, 1390
Moya, P. S., Navarro, R., Muñoz, V., & Valdivia, J. A. 2013, PhRvL, 111, 029001
Moya, P. S., Viñas, A. F., Muñoz, V., & Valdivia, J. A. 2012, AnGeo, 30, 1361
Ofman, L., & Viñas, A. F. 2007, JGR, 112, A06104
Ofman, L., Viñas, A., & Gary, S. P. 2001, ApJL, 547, L175
Ofman, L., Viñas, A. F., & Moya, P. S. 2011, AnGeo, 29, 1071
Press, W. H., Flannery, B. P., Teukolsky, S. A., & Vetterling, W. T. 1992, Numerical Recipes in Fortran 77: The Art of Scientific Computing (2nd ed.; Cambridge: Cambridge Univ. Press)
Smith, C. W., Isenberg, P. A., Matthaeus, W. H., & Richardson, J. D. 2006, ApJ, 638, 508
Smith, C. W., Matthaeus, W. H., Zank, G. P., et al. 2001, JGR, 106, 8253
Tu, C. Y., & Marsch, E. 1999, in AIP Conf. Proc. 471, Solar Wind Nine, ed. S. R. Habbal, R. Esser, J. V. Hollweg, & P. A. Isenberg (New York: Woodbury), 373
Vasquez, B. J., & Hollweg, J. V. 1999, in AIP Conf. Proc. 471, Solar Wind Nine, ed. S. R. Habbal, R. Esser, J. V. Hollweg, & P. A. Isenberg (New York: Woodbury), 167
Verscharen, D., Marsch, E., Motschmann, U., & Müller, J. 2012, PhRvE, 86, 027401
Viñas, A. F., & Goldstein, M. L. 1991, JPlPh, 46, 107
von Steiger, R., Zurbuchen, T. H., & McComas, D. J. 2010, GeoRL, 37, L22101
Wambecq, A. 1978, Compu, 20, 333
Winske, D., Yin, L., Omidi, N., Karimabadi, H., & Quest, K. 2003, in Lecture Notes in Physics, Vol. 615, Space Plasma Simulation, ed. J. Bchner, M. Scholer, & C. Dum (Berlin: Springer), 136
Yoon, P. H. 1992, PhFlB, 4, 3627
Yoon, P. H., Ryu, C.-M., & Rhee, T. 2003, PhPl, 10, 3881